Inorganic Chemistry

Article

pubs.acs.org/IC

# Puzzling Polymorphism of Layered $Ba(CoPO_4)_2$

Rénald David,[†] Houria Kabbour,[†] Alain Pautrat,[‡] and Olivier Mentré*[,†]

[†]Université Lille Nord de France, UMR 8181 CNRS, Unité de Catalyse et de Chimie du Solide (UCCS USTL), F-59655 Villeneuve d'Ascq, France

[‡]Laboratoire CRISMAT, UMR 6508 du CNRS, ENSICAEN et Université de Caen, 6 Bd Maréchal Juin, F-14050 Caen 4, France

Supporting Information

**ABSTRACT:** In this paper, we present the phase diagram and magnetic properties of the layered $Co^{2+}$-based compounds of formula $Ba(CoPO_4)_2$ for which the rhombohedral $\gamma$ form is well-known for its quasi-2D *XY* topology that is responsible for magnetization steps. The structural resolution of the new, room temperature-stable monoclinic $\alpha$ form shows similitude with the hydrated homologue $Ba(CoPO_4)_2{\cdot}H_2O$ and consists of the stacking between $[CoPO_4]^-$ sheets with chain subunits. We show by means of high temperature powder XRD and thermal analyses that the $\alpha$ form transforms into several polymorphs also exhibiting layered architectures upon heating. Three reversible transitions at 773, 893, and 993 K were observed from DTA which allowed us to define several forms as follows: $\alpha \rightarrow \alpha' \rightarrow \alpha'' \rightarrow \beta$. The crystallographic relationships between the several polymorphs and hydrate analogue are discussed. The $\alpha'$ and $\alpha''$ cell parameters involve a direct relationship with the $\alpha$ form, whereas the trigonal $\beta$ phase was fully solved and found isomorphic with the compounds $CaZn_2P_2O_8$ and $BaAl_2Si_2O_8$. The magnetic study of the $\alpha$ form shows an antiferromagnetic ordering at $T_N$ = 17 K, with spins canting below $T_N$. Then, the analysis of the magnetic interactions paths occurring within the layers evidence superexchange paths and additional supersuperexchange paths between the chains. This scheme leads to a hexagonal frustrated topology responsible for the canted spin structure in a 2D-topology of anisotropic $Co^{2+}$ magnetic ions.

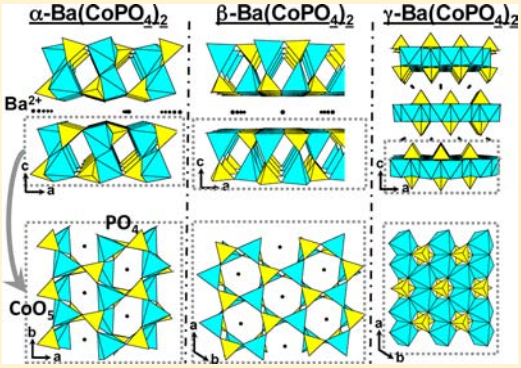


## INTRODUCTION

The layered compounds of general formula $Ba(MXO_4)_2$ (M = transition metal) have attracted great interest due to the various properties offered by the structure of their isolated honeycomb layers. Three different examples illustrate quite well the diversity of behaviors reached through the atom nature variation. (i) The cobaltite $Ba(CoAsO_4)_2$ is a good realization of a quasi-2D *XY* system in which the $Co^{2+}$ ions form a magnetically frustrated honeycomb lattice with magnetic moments mainly confined in the basal planes.[1] It contains almost ferromagnetic chains able to rotate without much of an energy cost that is responsible for magnetization steps below $T_N \sim 5.3$ K. (ii) The same topology with $Ni^{2+}$ ions in $Ba(NiVO_4)_2$ leads to a quasi-2D antiferromagnet that orders below $T_N \sim 50$ K and undergoes a Kosterlitz−Thouless transition at $T_{KT} \sim 43$ K compatible with a weakly anisotropic 2D Heisenberg character.[2] (iii) Finally, we have recently shown that $Ba(FePO_4)_2$ is the first 2D Ising ferromagnetic oxide with $T_C \sim 65$ K.[3] In addition to this variety of typical behaviors, $Ba(MXO_4)_2$ compounds form a rich playground because they can adopt several polymorphs depending on the synthesis conditions and thermal history. In the case of the honeycomb $Ba(CoXO_4)_2$ (designed as the $\gamma$ form hereafter) most of the studies focus on the arsenate compound (X = As, $\gamma$-$Ba(CoAsO_4)_2$ = $\gamma$-BCAO) due to difficulties of preparing $\gamma$-$Ba(CoPO_4)_2$ ($\gamma$-BCPO, also called the "high temperature form" in early reports[4]), exempt from its so-called "low temperature form" ($\alpha$-BCPO hereafter) whose structure is still not determined yet. In addition, $\gamma$-BCPO has been announced to undergo a phase transition into a 3D crystal structure isomorphous with $Ba(ZnPO_4)_2$ above 973 K. This form will be designated as the $\varepsilon$ form hereafter. In the X = As case, no form other than $\gamma$-BCAO was reported, this latter being easily obtained both as polycrystalline samples and as large single crystals grown by hydrothermal method.[5] It follows that the puzzling phase diagram of BCPO deserves particular attention by analogy to the BCAO case. This work was carried out in the search for new low *D* magnetic topologies of oxides.[6−8] For BCPO, we show by means of high temperature powder XRD, single crystal XRD, and thermal analyses that the situation is even more complicated than expected from the literature because two new $\alpha'$ and $\beta$ forms have been evidenced. The phase diagram seems dominated by layered architectures. The crystallographic relationships between the various polymorphs and related hydrates will be discussed, as well as the magnetic properties of $\alpha$-BCPO.

**Received:** April 11, 2013
**Revised:** July 2, 2013
**Accepted:** July 10, 2013
**Published:** July 22, 2013





dx.doi.org/10.1021/ic4009027 | Inorg. Chem. 2013, 52, 8732−8737

## EXPERIMENTAL SECTION

**Synthesis.** For the synthesis of polycrystalline $\alpha$-BCPO, a stoichiometric mixture of $BaCO_3$, $Co_3O_4$, and $(NH_4)_2HPO_4$ was ground in an agate mortar, placed in an alumina boat, heated to 900 °C for 72 h, and cooled by switching the furnace off. To obtain crystals, the synthesized powder was melted at 1500 K and quenched down to room temperature by removing the crucible from the furnace. This procedure avoids the production of the high temperature phase $\gamma$-BCPO, which appears as the major phase on slow cooling.[4]

**Single Crystal XRD.** Room temperature, single crystal XRD was carried out on a DUO-Bruker SMART apex diffractometer using Mo K$\alpha$ radiation. Crystals are typically twinned according to their pseudotrigonal structure, discussed later for the $\beta$-phase. Intensities were extracted and corrected for the Lorentz polarization factor through the SAINT program using the two orientation matrices of the predominant domains. Multiscan absorption corrections were applied using TWINABS.[9] The structure was solved using Superflip[10] using separated reflections of a single domain and refined with Jana 2006[11] by considering both isolated and composite intensities for the two domains (i.e., by the refinement of the domain1:domain2 ratio).

**Magnetic Measurements.** Data were measured on a PPMS Squid (Quantum Design) using powdered material pressed into a pellet. Typical measurements were performed using zero field cooling (ZFC) and field cooling (FC) procedures under a 0.1 T field. Magnetization versus $H$ was measured between +5 and −5 T at 2 K.

**Thermal Analyses.** Thermogravimetric experiments were carried out on a thermoanalyzer TGA 92 SETARAM under an air atmosphere using a ramp of 5 °C $min^{-1}$ from room temperature to 1173 K. X-ray thermodiffractometry was performed under 5 L $h^{-1}$ air flow in an Anton Paar HTK1200N on a D8 Advance Bruker diffractometer ($\theta$–$\theta$ mode, Cu K$\alpha$ radiation) equipped with a Vantec1 linear position sensitive detector (PSD). Each powder pattern was recorded in the range 10–80° (2$\theta$) (step $\Delta T$ = 25 °C, 30 min per scan, from 30 to 900 °C). The temperature ramp between two patterns was 0.08 °C $s^{-1}$.

**State of the Art on Reported BCPO Compounds.** The general phase diagram of $Ba(CoPO_4)_2$ (including our results combined with those previously reported[4,12]) is shown in Figure 1. In this paper, the different polymorphs mentioned in the literature are named according to the nomenclature detailed below:

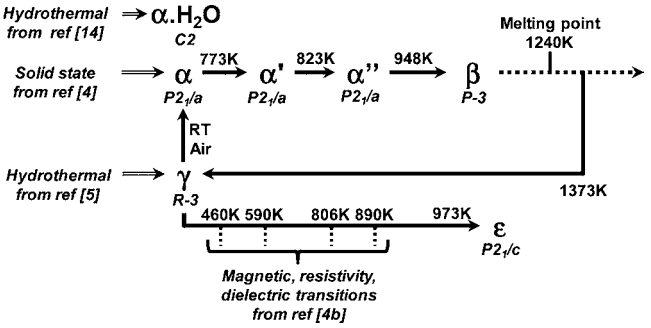


**Figure 1.** Phase relationships of $Ba(CoPO_4)_2$.

The $\alpha$ form is the so-called "low-temperature" form mentioned in previous papers.[4] In the latter, polycrystalline $\alpha$-BCPO was prepared by dissolution of precursors in nitric acid followed by an evaporation step and a high temperature treatment (1173 K) below the melting point (found at $T \sim 1240$ K). In earlier work, its XRD powder pattern was indexed in a monoclinic unit cell with lattice parameters of $a \sim 9.2$ Å, $b \sim 5.0$ Å, $c \sim 8.1$ Å, and $\beta \sim 87°$. However, in the absence of single crystals, the structure could not be solved. This compound was mainly used as a precursor to prepare the $\gamma$-rhombohedral form, denoted as the stable "high temperature" form after heating at 1373 K (well above the melting point) and cooling to room temperature (70 h cooling time). It was also reported that $\gamma$-BCPO is metastable and transforms into $\alpha$-BCPO after several weeks or months. Finally, it was also briefly reported[12] that upon heating, $\gamma$-BCPO shows a sequence of anomalies on both dielectric and magnetic properties at 460, 590, 806, and 890 K.[4b] Finally, it undergoes a transition around 973 K into three-dimensional $\varepsilon$-BCPO, which is was stated as isostructural with the three-dimensional (3D) $Ba(ZnPO_4)_2$ structural type.[13]

**Crystal Structure of $\alpha$-BCPO.** We have successfully prepared single phase polycrystalline $\alpha$-BCPO and single crystals as detailed in the Experimental Section. The structure resolution and refinement using single crystal data led to the following structure parameters: $a$ = 9.211(3) Å, $b$ = 5.0040(2) Å, $c$ = 8.0851(3) Å, $\beta$ = 92.737(1)°, space group $P2_1/a$, and the reliability factors $R$ = 3.42% and $Rw$ = 3.59%. The crystallographic data are summarized in Table 1, and atomic coordinates and selected bond distances are listed in Tables 2 and 3, respectively. $\alpha$-BCPO exhibits a 2D structure built from the stacking of infinite $(CoPO_4)^-$ sheets separated by $Ba^{2+}$ cations (Figure 2a). The shortest Co–Co distance between layers is 6.25 Å. The sheets are constituted of zigzag chains of corner sharing $Co^{2+}O_5$ distorted triangular bipyramids (Figure 3a) running along the $b$-axis. The shared corner is the atom O3 which belongs both to an equatorial $O_3$ triangle of a bipyramid and to the apical apex of the next one. The chains are interconnected into $(CoPO_4)^-$ sheets by $PO_4$ groups in a complex manner (i.e., $PO_4$ groups share one edge and one corner with two adjacent $CoO_5$ of the same chain) and share their last corner with a $CoO_5$ of the adjacent chain (Figure 3a).

**Table 1. Crystal Data and Refinement Characteristics for $\alpha$-$Ba(CoPO_4)_2$ at Room Temperature**

| | |
|---|---|
| Crystal Data ($T$ = 293 K) | |
| formula | $Ba(CoPO_4)_2$ |
| mol wt (g/mol) | 445.13 |
| symmetry | monoclinic |
| space group | $P2_1/a$ |
| unit cell (Å) and angle (deg) | a = 9.211(3) |
| | $b$ = 5.004(2) |
| | $c$ = 8.085(3) |
| | $\beta$ = 92.737(1) |
| vol (Å$^3$) | 372.23(2) |
| Data collection | |
| equipment | Bruker DUO |
| $\lambda$ (Mo K$\alpha$ (graphite monochromator); Å) | 0.7107 |
| density calc (g/cm$^3$) | 3.9703 |
| cryst dimens ($\mu$m) | 100 × 50 × 30 |
| color | blue |
| scan mode | $\omega$, $\varphi$ |
| $\theta$ (min–max) (deg) | 2.52–31.4 |
| $\mu$ (mm$^{-1}$ for $\lambda$ K$\alpha$ = 0.7107 Å) | 10.074 |
| $T_{min}/T_{max}$ | 0.82 |
| $R$(int) (%) | 5.8 |
| recording reciprocal space | $0 \le h \le 13$, $0 \le k \le 7$, $-11 \le l \le +11$ |
| number of measured reflections | 10 260 |
| no. of ind reflns/($I > 2\sigma(I)$) | 2695/2171 |
| Refinement | |
| no. of refined parameters | 63 |
| refinement method | least squares on $F$ |
| twin fraction $hkl$/(120° around $c^*$) | 0.6559(9)/0.3441(9) |
| weighting scheme | unit |
| R1($F$)[ $I > 2\sigma(I)$]/R1($F^2$) [all data], % | 3.43/4.5 |
| wR2($F^2$) [ $I > 2\sigma(I)$]/wR2($F^2$) [all data], % | 3.61/4.39 |
| GOF | 1.99 |
| max/min residual electronic density (e$^-$/ Å$^3$) | +2.74/−1.32 |
| $Z$ | 2 |


dx.doi.org/10.1021/ic4009027 | Inorg. Chem. 2013, 52, 8732–8737

**Table 2. Atomic Coordinates and Equivalent Isotropic Displacement Parameters (Å$^2$) for $\alpha$-Ba(CoPO$_4$)$_2$ (Single Crystal Data) and $\beta$-Ba(CoPO$_4$)$_2$ (XRD Powder Data at 900 K)**

| $\alpha$-Ba(CoPO$_4$)$_2$ ($P2_1/a$) | | | | | |
|---|---|---|---|---|---|
| atom | Wyck | $x$ | $y$ | $z$ | $U_{eq}$ |
| Ba | 2a | 0 | 0 | 0 | 0.0154(1) |
| Co | 4e | −0.70689(7) | 0.0663(1) | 0.34814(7) | 0.0141(1) |
| P | 4e | 0.3642(1) | −0.0054(2) | 0.2639(1) | 0.0106(2) |
| O1 | 4e | −0.2346(4) | 0.3530(7) | 0.1410(4) | 0.0213(9) |
| O2 | 4e | 0.5217(4) | 0.0504(8) | 0.2217(4) | 0.0223(10) |
| O3 | 4e | 0.3280(4) | 0.1126(6) | 0.4352(4) | 0.0185(8) |
| O4 | 4e | −0.1565(4) | 0.8062(7) | 0.2594(4) | 0.0241(10) |
| $\beta$-Ba(CoPO$_4$)$_2$ ($P\bar{3}$) | | | | | |
| atom | Wyck | $x$ | $y$ | $z$ | $U_{iso}$ [a] |
| Ba | 1a | 0 | 0 | 0 | 0.088(1) |
| Co | 2d | 1/3 | 2/3 | 0.6528(3) | 0.088(1) |
| P | 2d | 1/3 | 2/3 | 0.2551(4) | 0.088(1) |
| O1 | 6g | 0.4366(6) | 0.9731(6) | 0.2290(5) | 0.088(1) |
| O2 | 2d | 1/3 | 2/3 | 0.4302(6) | 0.088(1) |

[a]Atoms have been assigned to zero thermal parameters, and U overall was refined.

**Table 3. Selected Bond Lengths (Å) for $\alpha$-Ba(CoPO$_4$)$_2$ and $\beta$-Ba(CoPO$_4$)$_2$**

| $\alpha$-Ba(CoPO$_4$)$_2$ ($P2_1/a$) | | | | $\beta$-Ba(CoPO$_4$)$_2$ ($P\bar{3}$) | |
|---|---|---|---|---|---|
| Co | | Ba | | Co | |
| Co−O1 | 2.289(3) | Ba−O1 | 2 × 3.054(3) | Co−O1 | 3 × 1.917(4) |
| Co−O2 | 1.948(3) | | 2 × 2.748(3) | Co−O2 | 1.839(6) |
| Co−O3 | 2.007(3) | Ba−O2 | 2 × 2.878(4) | P | |
| | 2.061(3) | Ba−O4 | 2 × 2.776(4) | P−O1 | 3 × 1.427(3) |
| Co−O4 | 1.970(4) | | | P−O2 | 1.446(6) |
| P | | | | Ba | |
| P−O1 | 1.520(3) | | | Ba−O1 | 6 × 3.022(4) |
| P−O2 | 1.532(3) | | | | |
| P−O3 | 1.556(3) | | | | |
| P−O4 | 1.517(3) | | | | |

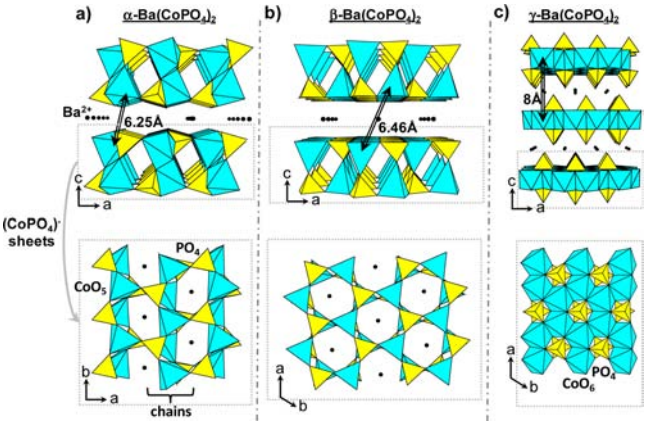


**Figure 2.** Description of the 2D structure of (a) $\alpha$-Ba(CoPO$_4$)$_2$, (b) $\beta$-Ba(CoPO$_4$)$_2$, and (c) $\gamma$-Ba(CoPO$_4$)$_2$.

This structure was very similar to that of the hydrated homologue, $\alpha$-BCPO·H$_2$O,[14] which contains a similar stacking of (CoPO$_4$·H$_2$O)$^-$ sheets (Figure 3). The absence of water molecules in the title polycrystalline sample has been confirmed by IR study, with the spectrum between 450 and 4000 cm$^{-1}$ showing (see Supporting Information, Figure S1) only vibration bands of the PO$_4$ groups (1100−950 cm$^{-1}$: $\nu_{ass}$ (stretching mode) and 625−500 cm$^{-1}$: $\delta_{ass}$ (bending mode)). XRD patterns of the hydrate and anhydrous

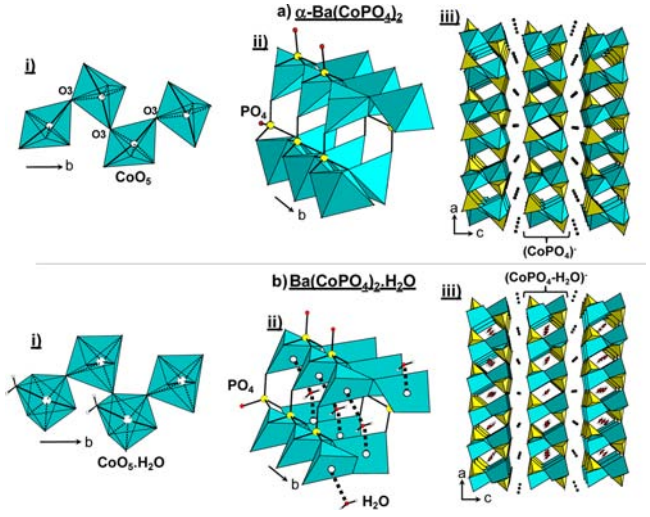


**Figure 3.** Comparison between (a) $\alpha$-Ba(CoPO$_4$)$_2$ and (b) Ba(CoPO$_4$)$_2$·H$_2$O structures considering (i) the chain, (ii) the arrangement between the chains, and (iii) the 2D stacking.

compounds were different and are given in Supporting Information Figure S2. After synthesis of the $\alpha$ form (powder) and air exposure for 3 months, we checked that the initial XRD powder pattern was preserved and perfectly matched the anhydrous form. The presence of the O$_w$ water molecule in the hydrate sheets creates CoO$_5$O$_w$ octahedra. It is such that the original chains were transformed into corner-sharing CoO$_5$OH$_2$ and were directly connected between each other by sharing O$_w$ corners (Figure 3b). Because of the stacking along $c$, the presence of a water molecule in the structure does not imply important changes; only the interlayer distance changes from 6.24 Å for $\alpha$-BCPO to 6.44 Å for the hydrated compound. An analysis of magnetic exchange paths in $\alpha$-BCPO and $\alpha$-BCPO·H$_2$O will be given in the last section of this paper.

**Thermal Behavior.** As already discussed, even though the structure of $\alpha$-BCPO remained unknown until our current work, it was designated as the "low temperature" form because it was observed from the slow cooling of molten BCPO. However, starting from the rhombohedral $\gamma$-BCPO 2D structure, a destabilization toward a 3D phase isostructural with Ba(ZnPO$_4$)$_2$ ($P2_1/c$) was reported.[12] Taking into account this puzzling scheme, we have studied the thermal stability of $\alpha$-BCPO by DTA to probe the possibility of new crystalline intermediates. The DTA curve highlights three reversible transitions at


dx.doi.org/10.1021/ic4009027 | Inorg. Chem. 2013, 52, 8732−8737

770, 890, and 990 K (see Figure 4c) between $\alpha \rightarrow \alpha' \rightarrow \alpha'' \rightarrow \beta$ forms, as shown in Figure 1, by endothermic discontinuities on

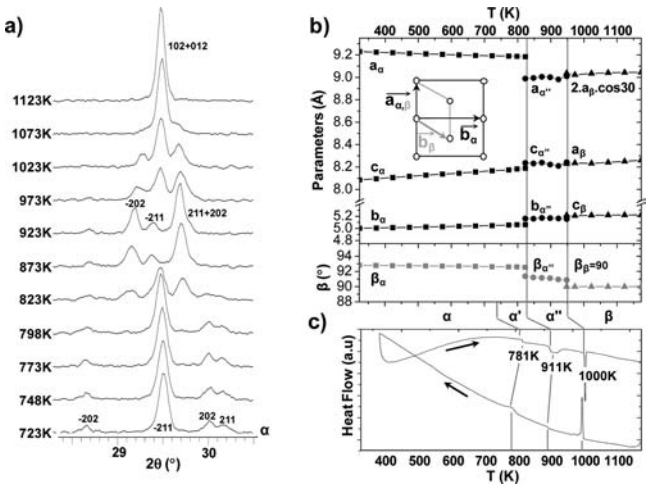


**Figure 4.** (a) Evolution of some reflections (in a determined $2\theta$ range) with the temperature showing evidence of $\alpha \rightarrow \alpha'' \rightarrow \beta$ transitions, (b) evolution of cell parameters with temperature and phase diagrams, and (c) DTA curves for $Ba(CoPO_4)_2$.

heating. For the determination of the associated crystal structures, X-ray thermodiffraction (XRT) was performed between room temperature and 1173 K (i.e., below the melting point). The temperature was slowly increased to 1173 K, although it was maintained constant at 50 K intervals for isothermal XRD data collection. Because of the continuous heating during DTA experiments (5 K/min) compared to discontinuous XRT, the observed transition temperatures are higher for DTA due to different kinetic parameters. Also, the XRT study (all patterns are given in Supporting Information Figure S3) highlights only two of the three phase transitions, as described below.

*$\alpha \rightarrow \alpha'$, $\alpha''$ Transitions.* The evidence for the $\alpha \rightarrow \alpha'$ transition was only evidenced on the DTA curve by a weak anomaly at 770 K, whereas the refined lattice parameters of the monoclinic $\alpha$-BCPO show a continuous evolution between 300 and 823 K (Figure 4b). The $b_\alpha$ and $c_\alpha$ parameters gradually increase, whereas $a_\alpha$ contracts on heating, probably to emulate the next $\alpha''$ phase, which is predominant at higher temperatures. In the absence of any clues for the $\alpha'$ phase by XRD, one could imagine that the transition is associated with a weak distortion of the original structure that is not visible with our standard XRD resolution. At 823 K, a distinct break of the lattice parameters (see Figure 4b) occurs that corresponds to the appearance of the $\alpha''$ phase. Indexations of the powder patterns have been attempted in various symmetries (monoclinic, orthorhombic, trigonal) but only a monoclinic cell matches (space group $P2_1/a$, $a$ = 8.2395(6) Å, $b$ = 5.1739(4) Å, $c$ = 9.0055(5) Å, and $\beta$ = 91.155(3)° at 873 K). In fact, as shown on the Figure 4a, the $\alpha \rightarrow \alpha', \alpha''$ transitions are not accompanied by the coalescence of peaks but by drastic shifts between them. It follows that these transitions correspond to rare cases of isosymmetric phase transitions. The fine analysis of reflection intensities shows drastic changes (see Figure 4a). For instance the intensity of the −211 reflection drastically decreases, whereas the −202 increases across the transition. These structure factor changes are likely due to the displacive rearrangement of the heavy $Ba^{2+}$ ions into 2D sheets to satisfy the hexagonal symmetry met at the next transition. However, we did not have a high temperature diagram of the $\alpha''$ phase fully exempt of the two bordering phases ($\alpha'$ or $\beta$) so that the structure resolution was not attempted.

*$\alpha'' \rightarrow \beta$ Transition.* At 973 K, a second discontinuous evolution of the refined cell parameters appears (see Figure 4c) together with a strong endothermic phenomenon on DTA. It corresponds to the appearance of the trigonal $\beta$ phase. Most probably, the $\alpha$ phase is metastable at high temperatures such that $\alpha'$, $\alpha''$, and $\beta$ are kinetically trapped metastable phases rather than equilibrium phases. The relationship between the ($a$, $b$) base of the trigonal $\beta$ phase and the monoclinic $\alpha$ phase is shown in the inset of the Figure 4b. It is such that numerically $a_\alpha \sim 2a_\beta \cos(30°)$, $b_\alpha = c_\beta$, and $c_\alpha = a_\beta = b_\beta$. This transition is associated with the coalescence of groups of reflections as shown for the $(-202, -211, +211, +202)_{\alpha''}$ multiplet leading to the unique 102 in the $\beta$ trigonal phase. The unit cell parameters refined at 1173 K in a primitive trigonal cell are $a$ = 5.222(1) Å and $c$ = 8.260(2) Å. A fine analysis of the parent $\alpha$-BCPO sheet structure (see Figure 2a) evidence a pseudo-$\bar{3}$ axis between metal ions. On this basis, using the FullProf suite program,[15] several trigonal models have been considered for the Rietveld refinement of the $\beta$ form. Subsequently, two reliable models were pointed out, both exhibiting a similar cationic arrangement related to the $\alpha$-type in space groups $P\bar{3}$ and $P\bar{3}m1$. Oxygen positions were located from Fourier-difference maps after refinement of the cationic coordinates. The best fit was obtained for the less symmetrical $P\bar{3}$ model ($\chi^2$ = 2.247%, $R_{Bragg}$ = 8.13%, $R_f$ = 15.8%, $R_p$ = 38.7% and $R_{w_p}$ = 13.7%) compared to the $P\bar{3}m1$ model ($\chi^2$ = 2.65%, $R_{Bragg}$ = 12.6%, $R_f$ = 18.3%, $R_p$ = 40.9% and $R_{w_p}$ = 14.9%). The XRD pattern after refinement is given in the Supporting Information (see Figure S4). The difference between the two models mainly concerns the oxygen positions that are relaxed out of mirror-related equivalent positions (see Supporting Information Figure S5 for a comparison between the two structural models). Concerning this refinement using high temperature XRD, we note that some problems persist, such as that P−O distances have been constrained to lie in the 1.4−1.5 Å range. Due to high individual thermal parameters for all atoms, we finally refined a single overall thermal parameter that is identical for each atom (given in Table 2). The final interatomic distances are given in the Table 3. The $Co^{2+}$ ions adopt a tetrahedral setting with quite short Co−O bonds (3 × 1.917(4) and 1.839(6) Å). The high temperature is probably at the origin of the stability of this distorted configuration adopted by $Co^{2+}$

The refined structural model consists of a 2D stacking of $(CoPO_4)^-$ sheets separated by $Ba^{2+}$ layers (see Figure 2b) similar to the $\alpha$-BCPO model, but the arrangement between the atoms is modified into regular rings of corner-sharing tetrahedra (see Figure 2b). To the best of our knowledge, this structure is isomorphous with two compounds from the literature: $CaZn_2P_2O_8$[16] and $BaAl_2Si_2O_8$,[17] also assigned to the $P\bar{3}$ space group. One can note that for $BaAl_2Si_2O_8$, a mixed Si/Al disorder has been highlighted by $^{29}Si$ NMR MAS spectrometry.[17] Such a phenomenon was not considered in our refinement due to the poor Co/P contrast by powder XRD in presence of heavy $Ba^{2+}$ ions.

**Magnetic Properties.** The temperature dependence of the magnetic susceptibility of polycrystalline $\alpha$-BCPO is shown in Figure 5a. Above $T \sim 25$ K, $\chi(T)$ obeys the Curie−Weiss law fitted with the

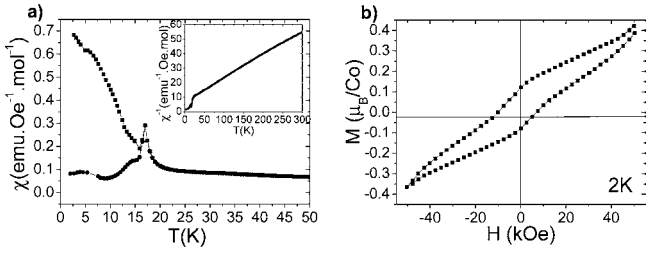


**Figure 5.** $\alpha$-$Ba(CoPO_4)_2$ magnetic measurements. (a) Temperature dependence of the magnetic susceptibility measured at 1000 Oe and corresponding inverse susceptibility (inset). (b) Magnetization as a function of applied field at 2 K.

parameters $\mu_{eff}$ = 7.084 $\mu$B/fu and $\theta_{CW}$ = −52.43 K. The high value of the effective magnetic moment, compared to the one calculated for two $Co^{2+}$ ($\mu_{eff}$ = 5.48 $\mu$B/fu, $S$ = 3/2, $g$ = 2) in the spin-only approximation, indicates that the $Co^{2+}$ exhibits a large orbital moment contribution as expected for this anisotropic magnetic ion. The negative Weiss constant indicates predominant antiferromagnetic exchanges between $Co^{2+}$ ions. The sharp peak observed at $T_N$ = 17


dx.doi.org/10.1021/ic4009027 | Inorg. Chem. 2013, 52, 8732−8737

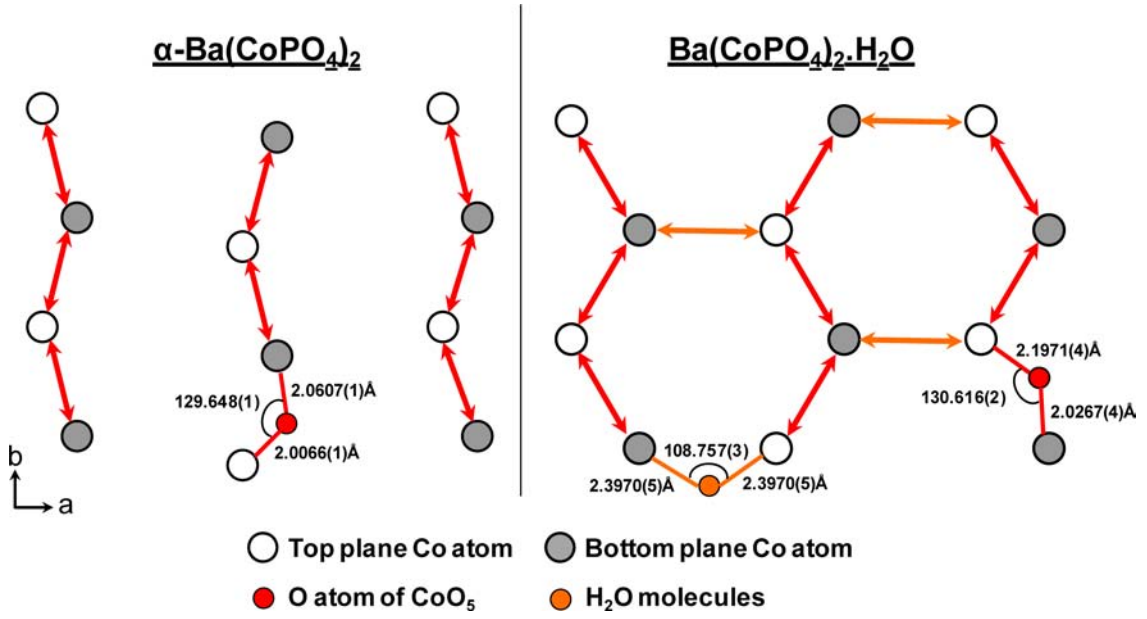


**Figure 6.** Description of the super exchange (SE) paths inside the layer of $\alpha$-$Ba(CoPO_4)_2$ (left) and $BaCo_2(PO_4)_2{\cdot}H_2O$ (right). (SSE are not shown for clarity.)

K shows the onset of antiferromagnetic (AF) ordering. Below 15 K, a significant ZFC/FC discrepancy occurs, which suggests the existence of a net uncompensated magnetic moment. The setting of this moment below $T_N$ is performed in several stages according to the anomalies observed on both ZFC and FC susceptibilities at 12.5 and 5 K. It could be proposed that a spin-flop like transition via canted states with noncollinear spin tilting upon cooling occurs. This behavior is favored by the strongly anisotropic magnetic behavior of $S = 3/2$ $Co^{2+}$ ions. The magnetization at 2 K shown on the Figure 5b does not show saturation up to $H = 5$ T, but a hysteresis cycle is opened with a remanent moment of 0.25 $\mu_B$/fu (0.125 $\mu_B$/Co) and a coercive field of 8 KOe. It should be noted that the magnetic cycle shown in Figure 5b is asymmetric and vertically shifted. This is very likely a minor loop effect caused by the unsaturated magnetization. Phenomena such as magnetization steps are well known for layered or chain-like cobalt oxides. For instance, in the layered $\gamma$-BCAO and $\gamma$-BCPO, the honeycomb lattice behaves as an *XY*-spin system with in-plane rotation of ferromagnetic chains due to a frustrated topology between them, which creates an Ms/3 plateau.[2] In-chain spin reversal was observed for $\alpha$-$CoV_2O_6$[18] and more recently in the modulated $BaCoX_2O_7$ (X = P, As)[19] but once more was driven by triangular/frustrated geometry between magnetic subunits. The most probable scenario for spontaneous spin-canting in $\alpha$-BCPO concerns exchanges within the layers. If one considers only Co−O−Co super exchanges (SE), Co−O ~ 2.0 Å, Co−O−Co ~ 130°, the 2D magnetic topology is as shown in Figure 6. Clearly, additional Co−O−O−Co supersuper exchanges (SSE) exist between the chains, leading to a hexagonal frustrated topology. This feature is better observed in the case of the hydrate analogue $\alpha$-BCPO·$H_2O$ where extra SE paths are mediated by water molecules. Canting would then occur from the competition between in-chain and interchain couplings in a frustrated context. At first sight, the exchanges between the chains can be regarded as weaker and antiferromagnetic, in agreement with the main AFM transition. More accurate analysis of the magnetic properties of $\alpha$-BCPO and its monohydrate using single crystals are currently in progress but are beyond the scope of this paper. From our preliminary study, at least we can say that the behavior is typical of low-dimensional cobalt systems, in good agreement with the layered structure that contains chain-subunits.

## CONCLUSION

The $Ba(CoPO_4)_2$ system phase diagram was investigated in this work, as well as the magnetic properties of the novel $\alpha$ form that is stable at room temperature. In comparison with homologue systems such as the arsenate $Ba(CoAsO_4)_2$, it shows a peculiar phase diagram with the apparition of several forms dominated by layered architectures. $\alpha$-$Ba(CoPO_4)_2$ consists of a 2D stacking of $(CoPO_4)^-$ sheets separated by $Ba^{2+}$ layers. The structures have strong similarities with the already reported hydrated form, which is also layered. We have established a complex sequence of reversible phase transitions $\alpha \rightarrow \alpha' \rightarrow \alpha'' \rightarrow \beta$, for which HT-XRD Rietveld refinement also confirms a layered topology for the $\beta$ form, whereas $\alpha'$ and $\alpha''$ remain from the parent $\alpha$ structure with some rearrangement in the $Ba^{2+}$ layers. Though the $\alpha'$, $\alpha''$, and $\beta$ forms most likely correspond to trapped metastable phases structurally related to the parent $\alpha$ crystal structure, it is striking that the full phase diagram of $Ba(CoPO_4)_2$ is dominated by layered structures. It could result from the large size of $Ba^{2+}$ cations, which likely play the role of "spacers" between compact $Co/PO_4$ layered subunits. Indeed, our prospection for new compounds in this chemical system almost systematically lead to compounds with low-dimensional magnetic units, such as in the layered but modulated $BaCoX_2O_7$ (X = P, As).[19] Concerning the $\alpha$-$Ba(CoPO_4)_2$ magnetic properties, the chains forming the $(CoPO_4)^-$ layers appear to possibly interact through Co−O−O−Co supersuper exchanges (SSE), creating in this way a hexagonal frustrated topology. In this context, the experimentally observed canting-spin structure could arise through the competition between in-chain and interchain couplings in a frustrated 2D scheme. Efforts are currently underway for the crystal growth of sufficiently large crystals of both BCPO and BCPO·$H_2O$ for an accurate comparison between their anisotropic magnetic properties and the role of the water molecules that play as an extra media of super exchanges in the monohydrate homologue


dx.doi.org/10.1021/ic4009027 | Inorg. Chem. 2013, 52, 8732−8737

## ■ ASSOCIATED CONTENT

### Supporting Information

IR spectrum of a polycrystalline sample of $\alpha$-$Ba(CoPO_4)_2$, comparison of XRD pattern of synthetized $\alpha$-$Ba(CoPO_4)_2$ after 3 months with $\alpha$-$Ba(CoPO_4)_2$ and $Ba(CoPO_4)_2{\cdot}H_2O$ simulated patterns, high temperature powder XRD pattern of $\alpha$-$Ba(CoPO_4)_2$ from 323 to 1173 K (25K steps), comparison between observed and calculated data for $\beta$-$Ba(CoPO_4)_2$ at 900 K, comparison between $P\bar{3}$ (left) and $P\bar{3}m1$ (right) models for $\beta$-$Ba(CoPO_4)_2$ structure at 900 K. This material is available free of charge via the Internet at http://pubs.acs.org.

## ■ AUTHOR INFORMATION

### Corresponding Author

*E-mail: olivier.mentre@ensc-lille.fr.

### Notes

The authors declare no competing financial interest.

## ■ ACKNOWLEDGMENTS

This work was carried out under the framework of the MAD-BLAST project supported by the ANR (Grant ANR-09-BLAN-0187-01). R.D. thanks the ENS-Lyon for his PhD grant. The Fonds Européen de Développement Régional (FEDER), CNRS, Région Nord Pas-de-Calais, and Ministère de l'Education Nationale de l'Enseignement Supérieur et de la Recherche are acknowledged for funding the X-ray diffractometers. Laurence Burylo and Nora Djellal are thanked for their precious technical help.

## ■ REFERENCES

(1) (a) Regnault, L. P.; Burlet, P.; Rossat-Mignod, J. *Physica B+C (Amsterdam)* **1997**, *86*, 660. (b) Regnault, L. P.; Rossat-Mignod, J. In *Magnetic Properties of Layered Transition Metal Compounds*; De Jongh, L. J., Ed.; Kluwer: Dordrecht, The Netherlands, 1990; pp 271−321.

(2) Heinrich, M.; Krug von Nidda, H. A.; Loidl, A.; Rogado, N.; Cava, R. J. *Phys. Rev. Lett.* **2003**, *91*, 137601.

(3) Kabbour, H.; David, R.; Pautrat, A.; Koo, H. J.; Whangbo, M. H.; André, G.; Mentré, O. *Angew. Chem., Int. Ed.* **2012**, *51*, 11745−11749.

(4) (a) Eymond, S.; Martin, C.; Durif, A. *Mater. Res. Bull.* **1969**, *4*, 595. (b) Dojcilovic, J.; Napijalo, M.; Novakovic, L.; Napijalo, M. J. *Mater. Chem. Phys.* **1990**, *26*, 339.

(5) Bircsak, Z.; Harrison, W. T. A. *Acta Crystallogr., Sect. C* **1998**, *54*, 1554.

(6) Aliev, A.; Huvé, M.; Colis, S.; Colmont, M.; Aziz, D.; Mentré, O. *Angew. Chem., Int. Ed.* **2012**, *37*, 9393.

(7) David, R.; Pautrat, A.; Kabbour, H.; Sturza, M.; Curelea, S.; André, G.; Pelloquin, D.; Mentré, O. *Chem. Mater.* **2011**, *23*, 5191.

(8) Mentré, O.; Kauffmann, M.; Ehora, G.; Daviero-Minaud, S.; Abraham, F.; Roussel, P. *Solid State Sci.* **2008**, *10*, 471.

(9) (a) *SAINT: Area-Detector Integration Software*; Siemens Industrial Automation, Inc.: Madison, WI, 1995. (b) Sheldrick, G. M., *Cell_Now-Twinabs*; University of Göttingen: Göttingen, Germany, 2003.

(10) Palatinus, L.; Chapuis, G. *J. Appl. Crystallogr.* **2007**, *40*, 786.

(11) Petricek, V.; Dusek, M.; Palatinus, L. *JANA2000: The Crystallographic, Computing System*; Institute of Physics: Praha, Czech Republic, 2000.

(12) Regnault, L. P. *Contribution à l'étude des excitations non linéaires dans des systèmes uni et bidmensionnels à anisotropie planaire*. PhD Thesis, Institut National Polytechnique de Grenoble, 1981.

(13) Schmidt, R.; Kniep, R. *Z. Kristallogr.* **1991**, *196*, 312.

(14) Xianhui, B.; Pingyun, F.; Stucky, G. D. *J. Solid State Chem.* **1997**, *131*, 387.

(15) Rodríguez-Carvajal, J. *Physica B* **1993**, *192*, 55 (program Fullprof available from http://www.ill.eu/sites/fullprof/).

(16) Czaya, R. *Acta Crystallogr., Sect. B* **1972**, *28*, 322.

(17) Kremenovic, A.; Norby, P.; Dimitrijevic, R.; Dondur, V. *Solid State Ionics* **1997**, *101*, 611.

(18) (a) Markkula, M.; Arévalo-López, A. M.; Attfield, J. P. *Phys. Rev. B* **2012**, *86*, 134401. (b) Lenertz, M.; Alaria, J.; Stoeffler, D.; Colis, S.; Diana, A.; Mentré, O.; André, G.; Porcher, F.; Suard, E. *Phys. Rev. B.* **2012**, *86*, 214428.

(19) David, R.; Kabbour, H.; Colis, S.; Pautrat, A.; Mentré, O. *J. Phys. Chem. C*, submitted for publication.